






SARS-COV-2 Spike Glycoprotein as Inhibitory Target for *In silico* Screening of Natural Compounds

Damilola A. Omoboyowa^{1,*} , Toheeb A. Balogun¹, Onyeka S. Chukwudozie² , Victor N. Nweze³ ,
Oluwatosin A. Saibu⁴ , Alausa Abdulahi⁵ 

¹ Department of Biochemistry, Adekunle Ajasin University, Akungba-Akoko, Ondo State, Nigeria; damilola.omoboyowa@aaua.edu.ng (D.A.O.), baloguntoheeb685@gmail.com (T.A.B.);

² Department of Cell Biology and Genetics, University of Lagos, Nigeria, solomononyeka84@gmail.com (O.S.C.);

³ Department of Biochemistry, University of Nigeria, Nsukka, Nigeria, nwezevictor@rocketmail.com (V.N.N.);

⁴ Department of Environmental Toxicology, Universitat Duisburg-Essen, NorthRhine-Westphalia, Germany, saioluwatosin@gmail.com (O.A.S.);

⁵ Department of Biochemistry, Ladoke Akintola University of Technology, Ogbomoso, Oyo State, Nigeria, alausaopeyemi0@gmail.com (A.A.);

* Correspondence: damilola.omoboyowa@aaua.edu.ng (D.A.O.);

Scopus Author ID 56086512700

Received: 26.02.2021; Revised: 23.03.2021; Accepted: 26.03.2021; Published: 7.04.2021

Abstract: Coronavirus disease (Covid-19) caused by SARS-Cov-2 has raised global health concerns without approved drugs to manage this life-threatening disease. This study aimed to predict the inhibitory potential of quercetin-3-o-rutinoside against SARS-Cov-2 spike glycoprotein. Targeting the SARS-Cov-2 Nucleocapsid spike glycoprotein (pdb id: 6m3m) is gaining importance. In this present study, the relationship between plant-derived natural drug and spike glycoprotein was predicted using *in silico* computational approach. The results were evaluated according to the glide (Schrodinger) dock score. Among the five (5) screened natural compounds, quercetin-3-o-rutinoside has the best docking score (-9.296) with the target. Molecular dynamic (MD) simulation analysis was performed for 1000ps to confirm the spike protein's stability behavior and quercetin-3-o-rutinoside complex. The MD simulation analysis validated the stability of quercetin-3-o-rutinoside in the spike protein binding pocket as a potent inhibitor. The pharmacokinetics screening of the natural compounds showed that quercetin-3-o-rutinoside possesses good oral bioavailability with no side effects.

Keywords: Covid-19; quercetin-3-o-rutinoside; spike protein; MD-simulation.

© 2021 by the authors. This article is an open-access article distributed under the terms and conditions of the Creative Commons Attribution (CC BY) license (<https://creativecommons.org/licenses/by/4.0/>).

1. Introduction

Coronavirus (Cov) belongs to the family coronaviridae [1], considered to be the largest RNA virus with genomes ranging from 27 to 32kb [2]. Coronavirus disease 2019 (Covid-19) is a major life-threatening disease worldwide due to its fast spreading [3]. Severe acute respiratory syndrome coronavirus 2 (SARS-Cov-2) has been reported as the cause of this pandemic [4]. The SARS-Cov-2 causes mainly severe acute and other complications in the heart, kidney, brain, and spleen, ultimately leading to disastrous effects in Covid-19 afflicted patients [5]. SARS-Cov-2 invades human cells through its spike proteins interaction with angiotensin-converting enzyme 2 (ACE 2) receptors. As a structural glycoprotein on the virion surface, the spike glycoprotein of coronavirus binds to the host cellular receptors, followed by fusion between the viral envelope and the cellular membrane [6]. Upon binding with the receptor, the protein changes its conformation from a pre-fusion to a post-fusion form [7].

The viral glycosylated spike protein comprises S1 and S2 subunits in the coronavirus, enabling them access into the host cell. The receptor-binding domain of the S1 subunit in SARS-CoV-2 cleaves to ACE2 led to the shed of the S1 subunit and subsequently triggered the cleavage of the S2 subunit by the host protease protein [8]. The biophysical and structural evidence shows that SARS-CoV-2 spike protein binds with ACE2 receptors with higher affinity [9]. Therefore, it targets small molecules to generate potential inhibitors of ACE2 interaction with the protein.

In silico studies of small molecules, including natural plant origin compounds have been screened and confirmed to inhibit this important target in SARS-Cov-2 [10,11] directly. However, drug development against coronavirus (Covid-19) has posed a great challenge to scientists. However, the virtual screening of databases and bioinformatics, and cheminformatics have improved the discovery of small molecules that bind to the selected target, which is the preliminary phase of drug design. Here, five natural compounds were screened, targeting the entry pathway of SARS-Cov-2 penetration into cells. The Quercetin and Kaempferol derivatives screened in this study are widely distributed plant flavonoids found in several vegetables, seeds, grains [12], and other plant parts. Studies suggested that these compounds promote antioxidant [13], anti-inflammatory [14], antiviral and immune-protective potentials [15].

Quercetin has been studied in various viral infection models due to its antiviral efficacy by inhibiting protease, polymerases, DNA gyrase suppression, and reverse transcriptase inhibition [12].

In this *in silico* study, molecular docking and molecular dynamics simulation were performed to ascertain the most potent inhibitory molecule against SARS-CoV-2 spike glycoprotein. The pharmacokinetics properties of these natural compounds were also explored to ascertain these compounds as therapeutic agents.

2. Materials and Methods

Glide tool from Schrodinger molecular drug discovery suite (version 2017-1) and AMBER 16 package was used for molecular docking and MD simulation, respectively, in this research.

2.1. Ligand preparation.

Five (5) natural compounds were used in this research were obtained from published works of literature, and they were used to prepare the library for this research. The phytochemicals' structures were downloaded in the Structure data format (sdf format) from the PubChem database (<https://pubchem.ncbi.nlm.nih.gov>). The ligands were prepared by the LigPrep module of Maestro 11.5 interfaces (Schrodinger suite 2017-1). The ligands were converted from 2D to 3D structures to include stereochemical, ionization, tautomeric variations, energy minimization, and optimized geometry, desalted and corrected for their chiralities and missing hydrogen atoms. The bond orders of these ligands were fixed, and the charged groups were neutralized. The ionization and tautomeric states were generated between pH of 7.0 \pm 2.0 using the Epik module. In the LigPrep module, the compounds were minimized by Optimized Potentials for Liquid Simulations (OPLS3) force field. A single low-energy ring confirmation per ligand was generated, and the optimized ligands were used for docking analysis [16].

2.2. Protein preparation.

SARS-CoV-2 nucleocapsid spike glycoprotein crystalized structure was retrieved from Protein Data Bank (<http://www.rcsb.org/pdb/home.do>) (pdb ID: 6M3M). Maestro11.5 interface was used to view the 3D structure. The protein was prepared according to Balogun *et al.* [16].

2.3. Nucleocapsid spike glycoprotein grid generation.

Using the module for generating receptor grid on maestro 11.5, the area of interaction between the nucleocapsid spike glycoprotein and ligands was generated. In the spike protein's binding box dimension, the docked pose's centroid was patterned in terms of the coordinates x, y, and z.

2.4. Molecular docking using glide tool.

Using the prepared spike glycoprotein and ligands, the molecules' molecular docking was carried out on maestro11.5 from Schrödinger 2017-1. The phytochemicals of *P. dulcis* were docked into the protein's active site according to extra precision mode (X-P) alongside a sampling of the ligands as none refine only. The ligand interaction tool was used to view the ligand interaction with the amino acid residues at the protein's binding pocket [16].

2.5. Pharmacokinetics screening of hit compounds.

The ADME toxicity depicts the absorption, distribution, metabolism, excretion, toxicity and elucidates the natural compounds' pharmacokinetics profiles. The ADME toxicity screening of the natural compounds was performed with the admetSAR prediction online tool (<http://lmmd.ecust.edu.cn:8000/>) [17].

2.6. Molecular dynamics simulations.

The molecular dynamics simulation was conducted at a simulation time of 10000 ps using the AMBER 16 package. The topology files of the superimposed complex were constructed using the in-house program of the package. The antechamber program was used to assemble the force fields for the receptor residues and ligand molecules, while for the construction of the biopolymers from the component residues and preparation of the force field, the LEaP plugin was used. The AMBER ff14SB [18] and gaff force field [19] were used for the receptor amino residue and the ligand complex. The electrostatic interactions are handled by a particle-mesh Ewald (PME) protocol, and long-range Lennard-Jones attractions are treated by a continuum model. This gives densities and cohesive energies of simple liquids that are in excellent agreement with more elaborate methods [20]. The distribution of the viral receptors and the compounds RMSD were displayed with histogram using the R package, and the associated hydrogen bonding receptor and hydrogen bonding acceptor between the ligands and viral receptors at each picosecond were calculated. Using one of the program plugins, such as the MDTraj [21], the nonnative contact was calculated and using the Bio3d, the residue cross-correlation was calculated [22]. For the trajectory analysis, parameters considered were radius of Gyration (Rg), Root Mean Square Deviation (RMSD), Fraction of Native Contacts (Q), Root Mean Square Fluctuation (RMSF), B-factor, Principal Component Analysis (PCA), dynamic cross-correlations analysis, hydrogen bond analysis, and energy calculations.

3. Results and Discussion

3.1. Molecular docking result.

The molecular docking analysis was performed for the prediction of potential inhibitory compounds against SARS-Cov-2 spike protein. Although all the screened compounds exhibited a good docking score (Figure 1), the literature search showed that quercetin had a history of antioxidant, anti-inflammatory, and antiviral potential [12], therefore, selected for further computational investigation. The choice of quercetin-3-o-rutinoside was further supported by the findings of Heinz *et al.* [23], who reported quercetin supplementation and upper respiratory tract infection in a randomized community clinical trial. The selective inhibition of quercetin-3-o-rutinoside against SARS-CoV-2 spike protein is probably due to the formation of six hydrogen bond interactions with spike glycoprotein (ALA-139, TRY-133, ARG-69, LYS-66, and GLY-126 (Figure 2).

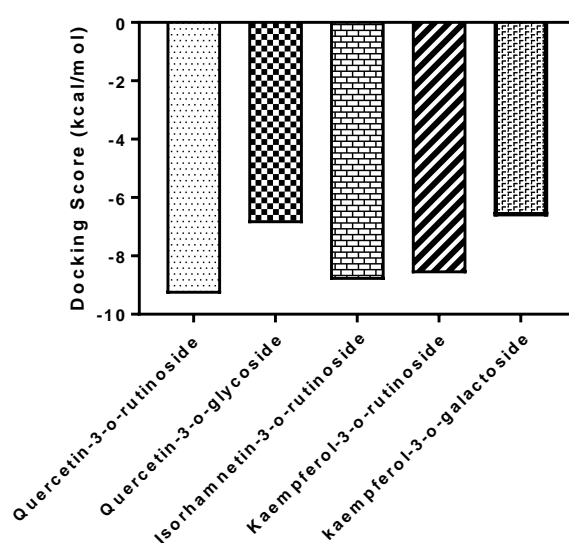


Figure 1. The binding affinity (kcal/mol) for the docking of the natural compounds against Nucleocapsid Spike Glycoprotein.

Table 1. Docking results of natural compounds against Nucleocapsid Spike Glycoprotein.

S/N	Entry Name	Dock score	Glide score	Glide model
1.	quercetin-3-o-rutinoside	-9.296	-9.308	-74.457
2.	isorhamnetin-3-o-rutinoside	-8.823	-8.834	-71.423
3.	kaempferol-3-o-rutinoside	-8.598	-8.610	-77.458
4.	quercetin-3-o-glucoside	-6.877	-6.888	0.000
5.	kaempferol-3-o-galactoside	-6.648	-6.660	-56.932

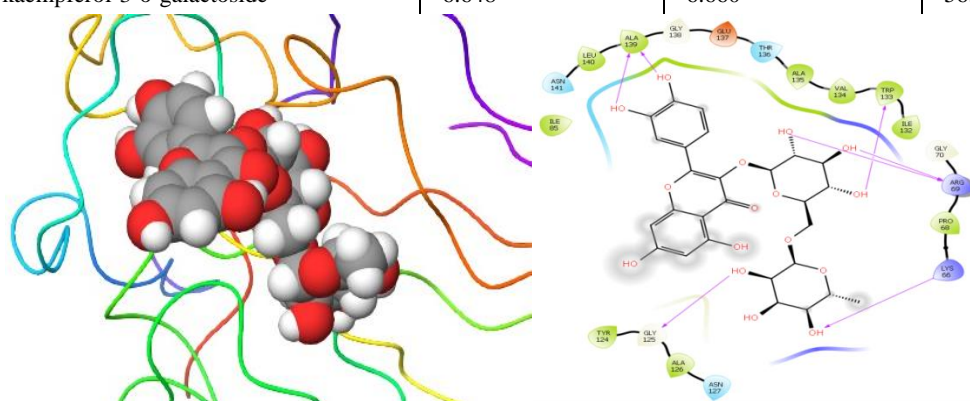


Figure 2. Protein-ligand interaction of quercetin-3-o-rutinoside against spike glycoprotein.

3.2. Pharmacokinetics profile of the natural compounds.

The *in silico* ADMET screening technique has proved reliable in predicting therapeutic agents' pharmacokinetic profiles [24]. Most readily available drugs are orally administered for their efficacy; they must be absorbed into the bloodstream [25]. Table 2 showed that all the natural compounds are human intestinal absorption (HIA) positive; these compounds can be absorbed into the bloodstream for systemic circulation. The failure of most promising drugs in the presence of barriers between blood and brain [26]. All the compounds under investigation cannot cross the barrier between blood and brain (BBB-). Therefore, the administration of these compounds cannot result in neurological disorders. The p-glycoprotein (p-gp) is an efflux membrane transported. It hinders the retention, permeability, and absorption of drugs that are its substrates, channeling them out of the cells. Table 2 showed that all the compounds are non-substrate of p-glycoprotein, hence, thrusting them out of the cell. The evaluation of therapeutic agents relies on their ability to inhibit or act as a substrate for CYP₄₅₀ isoforms, which help predict the disposition, efficacy, or toxicity of synergistic administration with known CYP₄₅₀ substrate [27]. From Table 2, all the natural compounds are non-substrate and non-inhibitor of CYP₄₅₀ 2C9, 2D6, 3A4, and 1A2 except kaempferol-3-o-rutinoside, which was observed as a substrate of CYP₄₅₀ 3A4. Therefore, co-administration of other drugs does not pose drug-drug interaction or toxicity. From Table 2, all the natural compounds are non-carcinogenic and non-toxic compounds.

Table 2. Pharmacokinetics profile of compounds.

Profile	quercetin-3-o-rutinoside	quercetin-3-o-glucoside	isorhamnetin-3-o-rutinoside	kaempferol-3-o-rutinoside	kaempferol-3-o-galactoside
Absorption					
BBB	-	-	-	-	-
HIA	+	+	+	+	+
CaCO ₂ P.	-	-	-	-	-
P-gp inhibitor	Non-substrate Non-inhibitor	Non-substrate Non-inhibitor	Non-substrate Non-inhibitor	Non-substrate Non-inhibitor	Non-substrate Non-inhibitor
Distribution					
Subcellular localization	Mitochondria	Mitochondria	Mitochondria	Mitochondria	Mitochondria
Metabolism					
CYP ₄₅₀ 2C9 substrate/inhibitor	Non-substrate Non-inhibitor	Non-substrate Non-inhibitor	Non-substrate Non-inhibitor	Non-substrate Non-inhibitor	Non-substrate Non-inhibitor
CYP ₄₅₀ 2D6 substrate/inhibitor	Non-substrate Non-inhibitor	Non-substrate Non-inhibitor	Non-substrate Non-inhibitor	Non-substrate Non-inhibitor	Non-substrate Non-inhibitor
CYP ₄₅₀ 3A4 substrate/inhibitor	Non-substrate Non-inhibitor	Non-substrate Non-inhibitor	Non-substrate Non-inhibitor	Substrate Non-inhibitor	Non-substrate Non-inhibitor
CYP ₄₅₀ 1A2 inhibitor	Non-inhibitor	Non-inhibitor	Non-inhibitor	Non-inhibitor	Non-inhibitor
Toxicity					
AMES toxicity	Non-AMES toxic	AMES toxic	Non-AMES toxic	Non-AMES toxic	Non-AMES toxic
Carcinogens	Non-carcinogen	Non-carcinogen	Non-carcinogen	Non-carcinogen	Non-carcinogen
Acute oral toxicity	III	III	III	III	III

Note: BBB: Blood-Brain Barrier; HIA: Human Intestinal Absorption; CaCO₂ P.: CaCO₂ Permeability; p-gp: P-glycoprotein; CYP₄₅₀: Cytochrome P₄₅₀.

3.3. Molecular dynamics of a protein-ligand complex.

The molecular analysis leads to the selection of quercetin-3-o-rutinoside, which showed the best inhibitory potential against SARS-Cov-2 spike protein. Biological activities may result in conformational changes in protein structure; also, the aqueous environment surrounding

protein plays a major role in protein-ligand complex interaction [7]. Hence, molecular dynamics simulation in a solvated environment was performed to investigate the conformational stability of quercetin-3-o-rutinoside binding to the binding domain of SARS-CoV-2 spike protein.

The RMSD for the spike protein was 2.5 Å, at a simulation time of 1ns, signifying the protein's stability during the simulation. At the same simulation time of 1ns, the RMSD of the ligand was 3.0 Å (Figures 3 and 4).

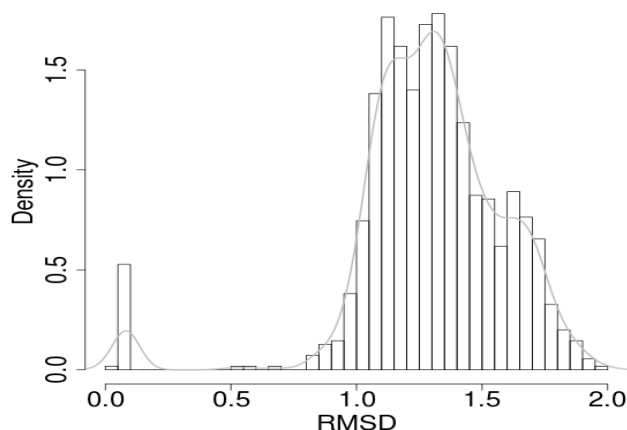


Figure 3. Generated RMSD histogram of the spike receptor.

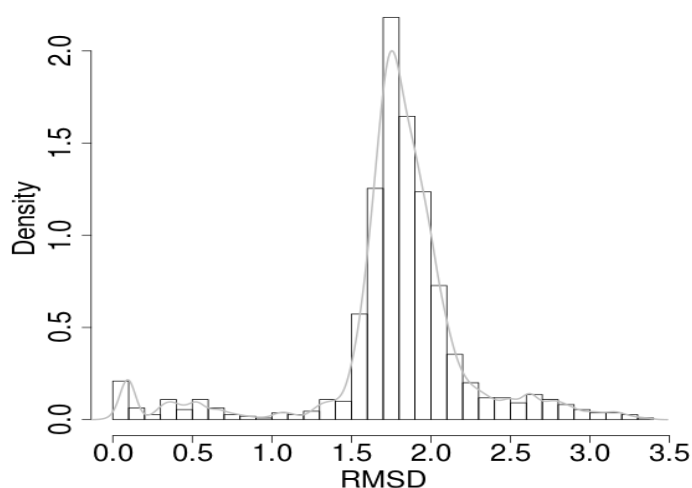


Figure 4. Generated RMSD plot for the ligand.

Given the docked complex between quercetin-3-o-rutinoside and SARS-CoV-2 spike protein, molecular dynamics (MD) simulations provide details about the atomic movements characterizing the interaction. With this, the stereochemical behavior of the docked complex is assessed. The Generated Root Mean Square Deviation (RMSD) plot indicates equilibrium or stability between the superimposed complex, which depends on the binding interaction and energy between the spike receptor and ligand.

Assessing the native contacts between the protein and quercetin-3-o-rutinoside, there were variations in the number of residual hydrogen bonds interacting with the quercetin-3-o-rutinoside at different simulation time scale (Figure 5). At the final simulation time of 1000 ps, four (4) hydrogen atoms were observed interacting with quercetin-3-o-rutinoside (Figure 6).

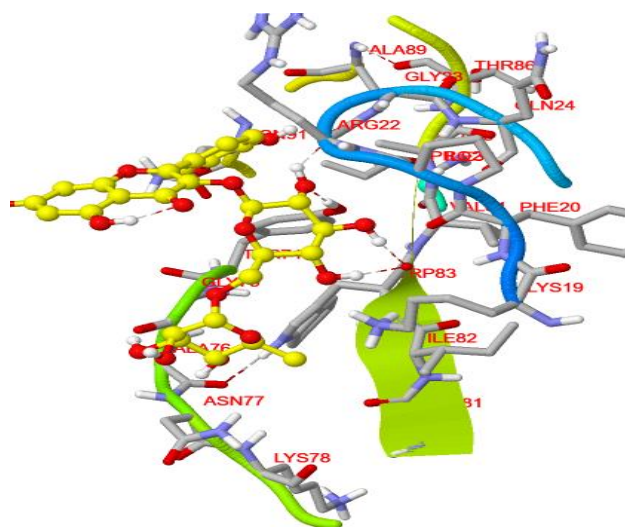


Figure 5. Native contacts between Spike protein residues and quercetin-3-o-rutinoside complex.

The RSMD crystallography resolution of the docked complex ranged from 1.5 to 2.9Å at a simulation time of 1000ps, which signifies that both relationships are linear (Figure 7). A resolution outside this range denotes that the complex can't be linear. The protein had a conformational change as indicated by the RSMD. The start of the ligand RSMD fluctuation was observed at a simulation time of 800 ps, which therefore continues till the end of the simulations.

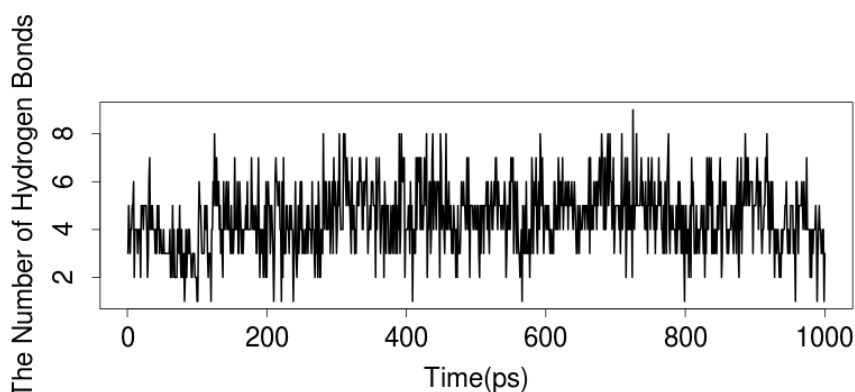


Figure 6. The number of hydrogen interactions between the ligand and the protein.

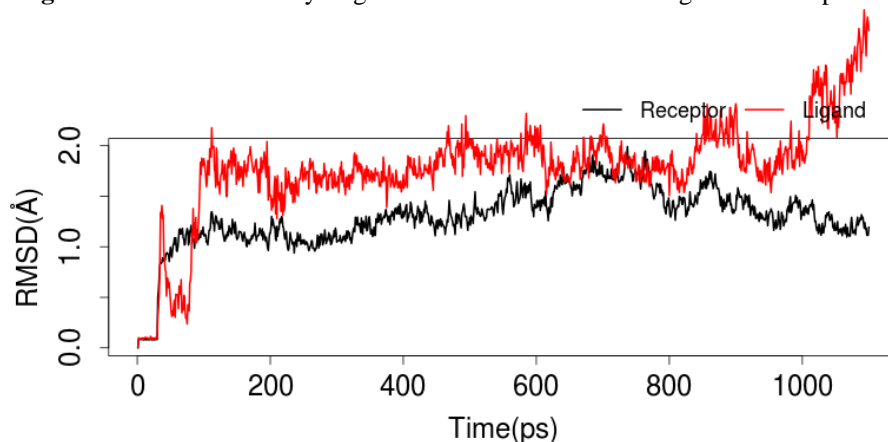


Figure 7. The RMSD of the viral spike receptor and ligand; Receptor: Nucleocapsid Spike Glycoprotein; Ligand: Quercetin-3-o-rutinoside.

This indicates that quercetin-3-o-rutinoside forms an unstable binding pose with the binding pocket of the protein target. The protein residue fluctuations after continuous linear attribute were observed at 600 ps, and at around the simulation time of 800 ps, stability was <https://biointerfaceresearch.com/>

sustained throughout the simulation period. In summary, the ligand was relatively stable, which implies that it forms a stable bond with the spike protein and has not diffused away from the protein's binding pocket.

The radius of gyration (R_g) was also considered to ascertain the changes in superimposed complex compactness. The radius of gyration measures the mass of atoms relative to the center of the complex's mass. There was an increase in R_g from the baseline trajectory from 200 ps simulation time, with an R_g complex of 14.3 nm, followed by a sharp decrease of 13.9 nm, at 700 ps simulation. At 1000 ps, the R_g complex was 14.5 nm, which implies the complex's compactness (Figure 8). To further analyze the atomic positional fluctuations of the residual RMSD, we considered the Root Mean Square Fluctuation (RMSF) of each residue. The fluctuation of each residue is calculated based on the CA atom of them. Residues at positions 30, 50, and 100 exhibited a higher fluctuation at 6Å, 6Å, and 8 Å, respectively (Figure 9).

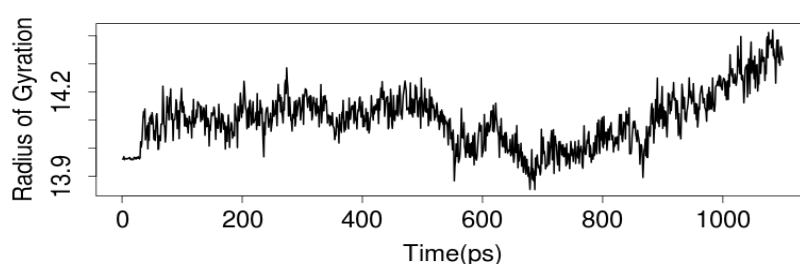


Figure 8. The Radius of Gyration (R_g) plot of the docked complex.

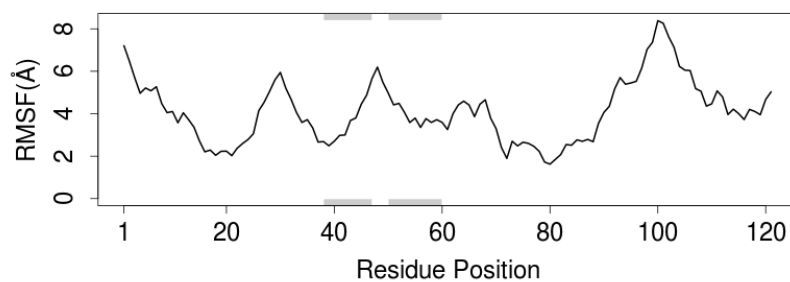


Figure 9. RMSF value of each residue. The secondary structure schematic is added to the figure's top and bottom margins (helices black, strands gray, and loops white).

3.3.1. Residues cross-correlation.

The atomic fluctuations of the docked complex system are correlated with one another, which can be evaluated by examining the magnitude of all the pairwise cross-correlation coefficients. The residues with negative correlations are few in the complex (Figure 10).

3.3.2. Energy calculations between the ligand and the protein receptor.

The spike protein residues that contribute to the decompose results comprising of the electrostatic energy as calculated by the MM force field (TELE), van der Waals contribution from MM (TVDW), total gas-phase energy (TGAS), the sum of non-polar and polar contributions to solvation (TGBSOL), final estimated binding free energy calculated from the terms above (TGBTOT), are displayed in a heat map. The unit of them is kcal/mol (Figure 11).

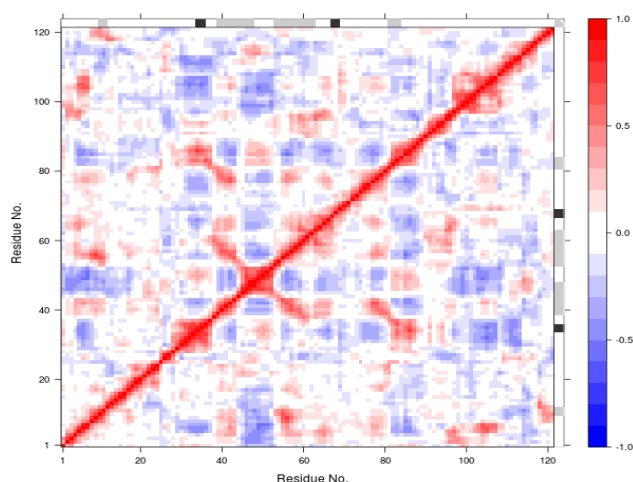


Figure 10. The cross residue correlation map of the atomic fluctuations of the spike receptor. The respective axis represents the residue indices on the Y-axis and the decomposed parameters on the X-axis. The secondary structure schematic is added to the top and right margins of the dynamical residue cross-correlation map (helices black, strands gray, and loops white).

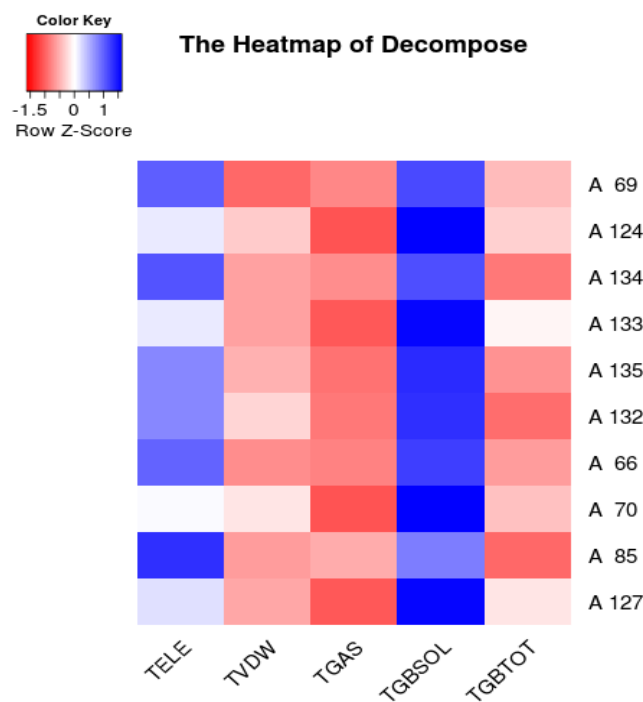


Figure 11. The residues that contribute to various decompose calculations. According to the energy ('TGBTOT'), the residues are ranked from top to bottom, and values are centered and scaled in the row direction shown with the heat map.

3.3.3. Principal cluster analysis (PCA).

The PCA tool quantitatively evaluates the collective motion and measures the moment direction [7,28]. The PCA and dynamic cross-correlation analysis were performed to evaluate the allosteric effect of SARS-CoV-2 spike protein under the ligand binding based on MD trajectory. This is to assess the direct and efficient mechanism for the modulation and regulation of cellular function in response to changes in small molecules' concentration. Therefore, 50% of the total variance of a given protein family structure can be captured by the principal components. This provides considerable insight into the nature of conformational differences. From the two clusters, the differential conformations can be studied. The value of

both clusters is 27.1%. Hence, the spike protein's PCA result and the ligand had no significant allosteric (Figures 9a and 9b).

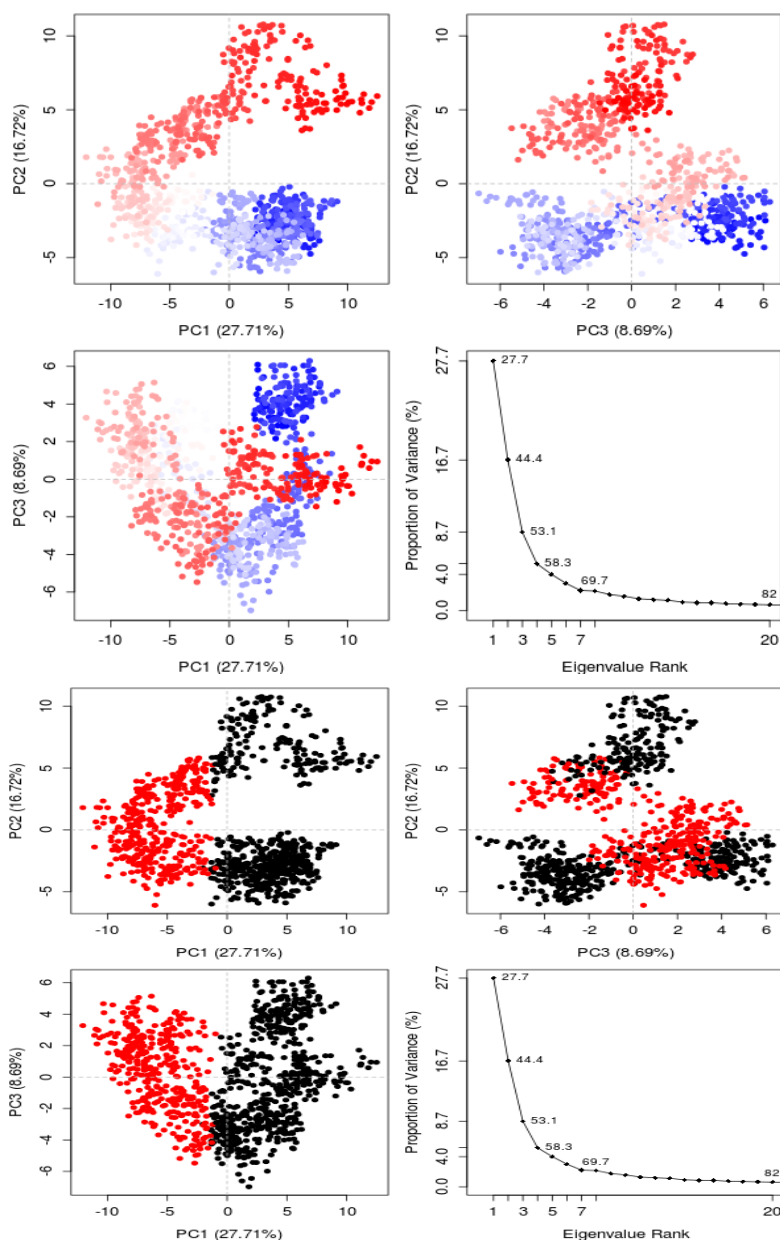


Figure 12. The PCA cluster of conformations and residues cross-correlation of the spike protein and ligand. The trajectory frames are highlighted in blue to white to red in time order. The N terminus is represented in blue, while the C-terminus is highlighted in red. The pink represents a pair of residues with a correlation coefficient >0.8 , and the blue lines depict a pair of residues with a correlation coefficient <-0.4 .

4. Conclusions

This work has identified quercetin-3-o-rutinoside as a direct inhibitor of SARS-CoV-2 spike protein through molecular docking analysis and prevents the interaction between human ACE-2 and SARS-CoV-2 spike protein which formed the key event of viral penetration and infection. The pharmacodynamics profile of quercetin-3-o-rutinoside depicted from the ADME toxicity reveals that this compound is a safe therapeutic agent, while the MD simulation predicted the stable bound or interaction quercetin-3-o-rutinoside with the binding pocket of SARS-CoV-2 spike protein.

Funding

This research received no external funding.

Acknowledgments

This research has no acknowledgment.

Conflicts of Interest

The authors declare no competing interests.

References

1. Pal, M.; Berhanu, G.; Desalegn, C. Severe Acute Respiratory Syndrome Coronavirus-2 (SARS-CoV-2): An Update. *Cureus* **2020**, *12*, e7423, <https://doi.org/10.7759/cureus.7423>.
2. Rahman, N.; Basharat, Z.; Yousuf, M.; Castaldo, G.; Rastrelli, L.; Khan, H. Virtual Screening of Natural Products against Type II Transmembrane Serine Protease (TMPRSS2), the Priming Agent of Coronavirus 2 (SARS-CoV-2). *Molecules* **2020**, *25*, 2271, <https://doi.org/10.3390/molecules25102271>.
3. Kadioglu, O.; Saeed, M.; Johannes, G. H.; Efferth, T. Identification of novel compounds against three targets of SARS CoV-2 coronavirus by combined virtual screening and supervised machine learning. [Preprint]. *Bull World Health Organ E-pub* **2020**, <http://dx.doi.org/10.2471/BLT.20.255943>.
4. Omotuyi, I. O.; Nash, O.; Ajiboye, B. O.; Metibemu, D. S.; Oyinloye, B. E.; Adelakun, N. S.; Hurdalay, R.; Aruleba, R. T.; Kappo, A. P. Darunavir Disrupts Critical Nodes in Metastable 2019-nCoV-RBD/ACE-2 Complex. [Preprint]. **2020**, <https://doi.org/10.20944/preprints202003.0125.v1>.
5. Madjid, M.; Safavi-Naeini, P.; Solomon, S. D.; Vardeny, O. Potential Effects of Coronaviruses on the Cardiovascular System: A Review. *JAMA Cardiol* **2020**, *5*, 831-840, <https://doi.org/10.1001/jamacardio.2020.1286>.
6. Zhang, Y.; Zheng, N.; Haoc, P.; Caod, Y.; Zhonga, Y. A molecular docking model of SARS-CoV S1 protein in complex with its receptor, human ACE-2. *Comp Biol and Chem* **2005**, *29*, 254-257, <https://doi.org/10.1016/j.compbiolchem.2005.04.008>.
7. Pandey, P.; Rane, J. S.; Chatterjee, A.; Kumar, A.; Khan, R.; Prakash, A.; Ray, S. Targeting SARS-CoV-2 spike protein of COVID-19 with naturally occurring phytochemicals: an in silico study for drug development. *Journal of Biomol Struc and Dyn* **2020**, <https://doi.org/10.1080/07391102.2020.1796811>.
8. Hoffmann, M.; Kleine-Weber, H.; Schroeder, S.; Kruger, N.; Herrler, Erichsen, S. SARS-CoV-2 Cell Entry Depends on ACE2 and TMPRSS2 and Is Blocked by a Clinically Proven Protease Inhibitor. *Cell* **2020**, *181*, 271-280, <https://doi.org/10.1016/j.cell.2020.02.052>.
9. Patel, D.; Chirag, N. S.; Prasanth, K.; Pandya, D.; Himanshu, A.; Rawal, D.; Rakesh, M. Identification of Potential Binders of the SARS-Cov-2 Spike Protein via Molecular Docking, Dynamics Simulation and Binding Free Energy Calculation. [Preprint]. *ChemRxiv* **2020**, <https://doi.org/10.26434/chemrxiv.12278588.v1>.
10. Zhang, D.; Wu, K.; Zhang, X.; Deng, S.; Peng, B. In silico screening of Chinese herbal medicines with the potential to directly inhibit 2019 novel coronavirus. *Journal of Integ Med* **2020**, *18*, 152-158, <https://doi.org/10.1016/j.joim.2020.02.005>.
11. Chen, G.; Yao, T.; Ahmed, A.; Pan, Y.; Yang, J.; Wu, Y. The discovery of potential natural products for targeting SARS-CoV-2 spike protein by virtual screening. [Preprint]. *BioRxiv* **2020**, <https://doi.org/10.1101/2020.06.25.170639>.
12. Biancatelli, R. M. L.; Berrill, M.; Catravas, J. D.; Marik, P. E. Quercetin and Vitamin C: An Experimental, Synergistic Therapy for the Prevention and Treatment of SARS-CoV-2 Related Disease (COVID-19). *Front Immunol* **2020**, *11*, 1451, <https://doi.org/10.3389/fimmu.2020.01451>.
13. Robaszekiewicz, A.; Balcerczyk, A.; Bartosz, G. Anti-oxidative and pro-oxidative effects of quercetin on A549 cells. *Cell Biol Int* **2007**, *31*, 1245-50, <https://doi.org/10.1016/j.cellbi.2007.04.009>.
14. Nair, M. P.; Kandaswami, C.; Mahajan, S.; Chadha, K. C.; Chawda, R.; Nair, H. The flavonoid, quercetin, differentially regulates Th-1 (IFN) and Th-2 (IL4) cytokine gene expression by normal peripheral blood

- mononuclear cells. *Biochim Biophys Acta* **2002**, *1593*, 29–36, [https://doi.org/10.1016/s0167-4889\(02\)00328-2](https://doi.org/10.1016/s0167-4889(02)00328-2).
15. Uchide, N.; Toyoda, H. Antioxidant therapy as a potential approach to severe influenza-associated complications. *Molecules* **2011**, *16*, 2032–2052, <https://doi.org/10.3390/molecules16032032>.
 16. Balogun, T. A.; Omoboyowa, D. A.; Saibu, O. A. *In silico* Anti-malaria Activity of Quinolone Compounds against *Plasmodium falciparum* Dihydrofolate Reductase (pfDHFR). *International Journal of Biochemistry Research & Review*, **2020**, *29*, 10-17, <https://doi.org/10.9734/IJBCRR/2020/v29i830208>.
 17. Akinloye, O. A.; Akinloye, D. I.; Onigbinde, S. B.; Metibemu D. S. Phytosterols demonstrate selective inhibition of COX-2: In-vivo and in-silico studies of *Nicotiana tabacum*. *Bioorganic Chem*, **2020**, *102*, 104037, <https://doi.org/10.1016/j.bioorg.2020.104037>.
 18. Maier, J.A.; Martinez, C.; Kasavajhala, K. ff14SB: improving the accuracy of protein side chain and backbone parameters from ff99SB. *J Chem Theory Comput* **2015**, *11*, 3696–3713, <https://doi.org/10.1021/acs.jctc.5b00255>.
 19. Wang, J.; Wolf, R.M.; Caldwell, J.W.; Kollman, P.A. Development and testing of a general amber force field. *J Comput Chem* **2004**, *25*, 1157–1174, <https://doi.org/10.1002/jcc.20035>.
 20. Horn, H.W.; Swope, W.C.; Pitara, J.W.; Madura, J.D.; Dick, T.J.; Hura, G.L. Head-Gordon, T.J. Development of an improved four-site water model for biomolecular simulations: TIP4P-Ew. *Chem Phys* **2004**, *120*, 9665-9667, <https://doi.org/10.1063/1.1683075>.
 21. McGibbon, R. T.; Beauchamp, K. A.; Harrigan, M. P. MDTraj: a modern open library for the analysis of molecular dynamics trajectories. *Biophys J* **2015**, *109*, 1528–1532, <https://doi.org/10.1016/j.bpj.2015.08.015>.
 22. Grant, B. J.; Rodrigues, A. P.; ElSawy, K. M. Bio3d: an R package for the comparative analysis of protein structures. *Bioinform* **2006**, *22*, 2695–2696, <https://doi.org/10.1093/bioinformatics/btl461>.
 23. Heinz, S.A.; Henson, D.A.; Austin, M.D.; Jin, F.; Nieman, D.C. Quercetin supplementation and upper respiratory tract infection: A randomized community clinical trial. *Pharmacological Research* **2010**, *62*, 237–242, <https://doi.org/10.1016/j.phrs.2010.05.001>.
 24. Sabu, V.; Peter, J.; Bai, A. I.; Nair, S.; Krishnan, S.; Suja, L. P.; Helen, A.; Pillai, G. R. Combinatorial Action of Triterpenoid, Flavonoid, and Alkaloid on Inflammation. *Nat Prod Comm* **2019**, 1–9, <https://doi.org/10.1177/1934578X19868877>.
 25. Yan, A.; Wang, Z.; Cai, Z. Prediction of human intestinal absorption by GA feature selection and support vector machine regression. *Int J Mol Sci* **2008**, *9*, 1961–1976, <https://doi.org/10.3390/ijms9101961>.
 26. Bors, L. A.; Erdo, F. Overcoming the Blood–Brain Barrier. Challenges and Tricks for CNS Drug Delivery. *Sci Pharm* **2019**, *87*, 6, <https://doi.org/10.3390/scipharm87010006>.
 27. Zhou, S. Drugs Behave as Substrates, Inhibitors and Inducers of Human Cytochrome P450 3A4. *Curr Drug Metab* **2008**, *9*, 310, <https://doi.org/10.2174/138920008784220664>.
 28. Sarma, P.; Shekhar, N.; Prajapat, M.; Avti, P.; Kaur, H.; Kumar, S.; Singh, S.; Kumar, H.; Prakash, A.; Dhibar, D. P.; Medhi, B. In-silico homology assisted identification of inhibitor of RNA binding against 2019-nCoV N-protein (N terminal domain). *Journal of Biomolecular Structure and Dynamics* **2020** 1–9, <https://doi.org/10.1080/07391102.2020.1753580>.